Unraveling the mechanism of photo-induced surface enhanced Raman scattering on ZnO/Au thin films

Van Tan Tran[1], Minh Phuong Le[1], Nguyen Hai Pham[1], Viet Tuyen Nguyen[1*], Thi Hong Pham[2], Cong Doanh Sai[1], Quang Hoa Nguyen[1], Van Thanh Pham[1], Thanh Binh Nguyen[1], Trong Tam Nguyen[3], An Bang Ngac[1], Oscar Martínez Sacristán [4], Thi Ha Tran[5*]

[1]Faculty of Physics, University of Science, Vietnam National University, Hanoi, 334 Nguyen Trai, Thanh Xuan, Hanoi, Vietnam

[2] Nano Energy Center, University of Science, Vietnam National University, Hanoi, 334 Nguyen Trai, Thanh Xuan, Hanoi, Vietnam

[3]Department of Physics, Faculty of Basic – Fundamental Sciences, Vietnam Maritime University, 484 Lach Tray, Le Tran District, Hai Phong, Viet Nam

3GdS-Optronlab group, Condensed Matter Physics Department , , University of Valladolid. Edificio LUCIA, 47019 Valladolid (Spain)

[5]Hanoi University of Mining and Geology, 18 Vien Street, Duc Thang Ward, Bac Tu Liem, Hanoi.

*nguyenviettuyen@hus.edu.vn (V.T. Nguyen); tranthiha@humg.edu.vn (T.H. Tran);

Abstract:

Surface-enhanced Raman scattering (SERS) is a powerful technique for detecting pollutants. Recent studies have shown that the sensitivity of SERS can be further improved by using appropriate light excitation before or during Raman measurements, a phenomenon known as photo-induced enhanced Raman scattering (PIERS). In this study, we developed a highly sensitive SERS substrate by fabricating a ZnO/Au thin film using radio frequency magnetron sputtering and post-annealing processes. The resulting substrate exhibited high crystallinity and enhanced sensitivity for pollutant detection.

The study found that in situ UV excitation significantly enhanced the Raman signal, up to 5.5 times more efficiently than the traditional SERS technique. The excitation process was reversible, allowing for a quick recovery of the Raman intensity to its initial level when the UV excitation was turned off. This relaxation process is attributed to the recombination of electrons and holes.

Keywords: ZnO thin films; Au nanoparticles; sputtering; surface enhanced Raman scattering (SERS); Photo induced enhanced Raman scattering (PIERS); UV excitation.

1. Introduction

Surface-enhanced Raman spectroscopy (SERS) is a highly sensitive technique capable of detecting trace amounts of substances for use in a variety of fields, including environmental monitoring, food safety, and life sciences [1]. Previous reports have shown that SERS originates from the inelastic light scattering of analyte molecules on the surface of metal nanostructures[2–4]. The enhancement of SERS involves two main mechanisms: electromagnetic (EM) enhancement and chemical (CM) enhancement. EM enhancement results from localized surface plasmon resonances (LSPR) due to the metal nanoparticles, which leads to significant SERS enhancement [2,4–6]. CM enhancement is the result of charge transfer between metal nanoparticles and the molecules of the analyte [5–8].

The two mechanisms can not be separated clearly but they work together to produce the overall

SERS effect. Despite of potential applications, only few SERS based products have been commercialized due to the difficulty in achieving high enough uniformity and stability. Hence, seeking for novel nanomaterials and optimizing material morphology to attain highest total SERS enhancement factor (EF) have attracted a lot of attention. However, there has been less room for material optimization thanks to deep and wide research of scientists in this area.

In recent years, alternative approaches have been proposed to improve SERS signal. Instead of focusing on the material itself, the scientists pay more efforts on optimizing the measurement process. Some studies have shown that if the sample is stimulated with a suitable light before or during Raman measurement, SERS signal can be enhanced greatly [5,9–11]. Such effect is known as photo induced enhance Raman scattering (PIERS). Although there have been a number of studies on PIERS, the underlying physics is not clearly understood due to the inherent complexity of SERS in association with photo-excitation effects.

Moreover, most of current studies have focused on the treatment of SERS substrates by UV radiation prior to Raman measurement, where the Raman enhancement is attributed to the generation of oxygen vacancies on the surface of ZnO nanostructures[12–16]. In this paper, we present the results of preparation of Au nanoparticles on ZnO thin films by sputtering method. The as-prepared structures are sensitive SERS substrates. The results also show that Raman signal can be efficiently enhanced further under in situ UV excitation. The study suggests an alternative mechanism of PIERS related to charge transfer process rather than oxygen vacancy generation. The physics nature of PIERS was revealed by both experiment and simulation.

2. Experiment

Glass slides with sizes of 10 mm ×10 mm ×1 mm were used as substrates for thin film deposition. The substrates were ultrasonically cleaned in acetone, ethanol and DI water in sequences. The substrates were rinsed with DI water and then blown dried by nitrogen gun. Mini sputter ULVAC (Japan) was used to deposit ZnO thin films on glass substrates. The chamber was first evacuated to a vacuum of $3\ 10^{-6}$ Pa, then Ar gas was introduced into the chamber to maintain the pressure at 1 Pa. Sputtering was performed with a power of 175 W and the sputtering time was fixed at 20 min. Substrate heating was not applied during sputtering.

In the second step, a layer of Au was deposited on top of the previously synthesized ZnO thin film by DC sputtering (JEOL JFC - 1200). Sputtering time was 30 s while sputtering current was maintained at 20 mA. Finally, the ZnO/Au thin film was annealed at 300 ºC for 2 h.

PANalitycal Empyrean X-ray diffractometer using Cu Kα = 1.54056 Å radiation was utilized to investigate the structure of the fabricated samples. Surface morphology of the samples was investigated by JEOL's scanning electron microscope (JSM – IT100). The transmittance and absorbance spectra of the thin films were collected on a Shimadzu UV - VIS (UV - 2450) spectrophotometer. SERS and PIERS effects were investigated using Horiba Jobin Yvon's LabRAM HR 800 Raman spectrometer with a 632.8 nm He-Ne laser source for excitation of the samples. Methylene blue reagent (MB) with different concentrations was used as Raman probe. A fixed volume of 50 μl of MB was dropped onto the samples. Raman measurements were performed after the samples were naturally dried. To investigate the PIERS effect, the samples were illuminated by a UV LED (wavelength of 365 nm and a power of 1 mW) from a tilted angle of 45° with respect to vertical direction during Raman measurement. The distance from the UV LED to the sample surface is 10 cm. The power density on the sample surface was estimated to be 0.2 mW/cm^2. Normal SERS and PIERS spectra were collected at the same point on the sample to verify the contribution of the UV excitation to the Raman enhancement.

3. Results and discussion

X-ray diffraction patterns of ZnO and ZnO/Au thin films are shown in Fig. 1. It can be seen that the obtained ZnO thin film has a high crystallinity with preferred orientation in the (002) direction. All the diffraction peaks match well with the JCPDS Card No. 36–1451 of hexagonal wurtzite structure of ZnO. The estimated lattice constants of the ZnO thin films are: a = 0.326 nm; c = 0.521 nm. These lattice parameters are in good agreement with the values reported in the literature for hexagonal ZnO [17]. Additional peaks observed in the XRD pattern of ZnO/Au samples can be indexed to those of Au.

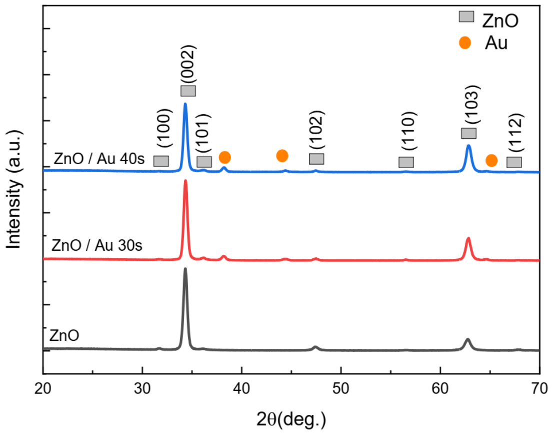

Fig. 1. X-ray diffraction patterns of ZnO and ZnO/Au thin films

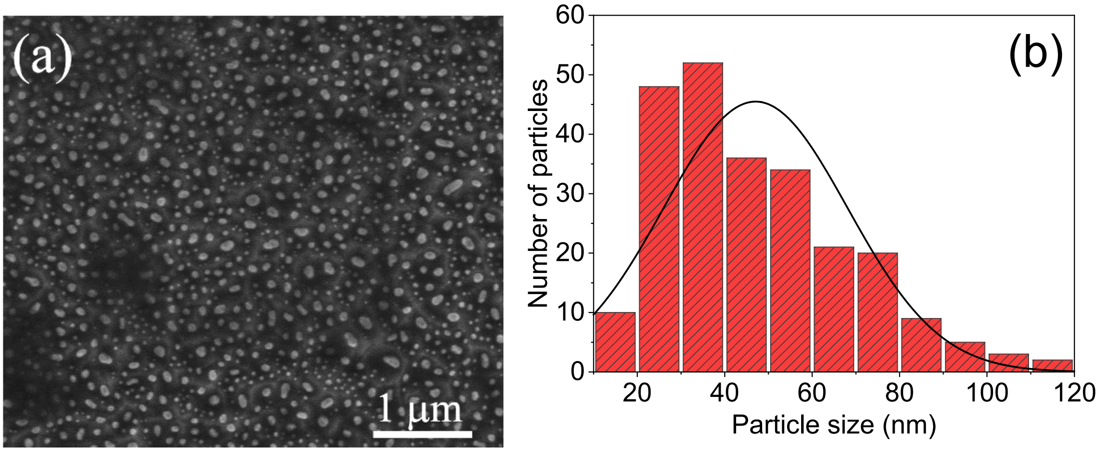

Fig. 2. (a) SEM images of the ZnO/Au thin films ; (b) Size distribution of the Au nanoparticles on ZnO thin films .

Fig. 2a is a SEM image of the ZnO/Au thin films annealed at 300 °C in 2h. It can be seen that annealing process transformed Au thin films into nanoparticles of high density. Size distribution of Au nanoparticles was statistically analyzed using ImageJ software, Fig. 2b. The statistic, performed over 240 particles, shows an average particle size of 47 nm. EDS spectrum in Fig. 3 shows that the ZnO/Au thin film is composed only of Zn, O and Au elements. It should be noted that the signal of Na comes from the glass substrate.

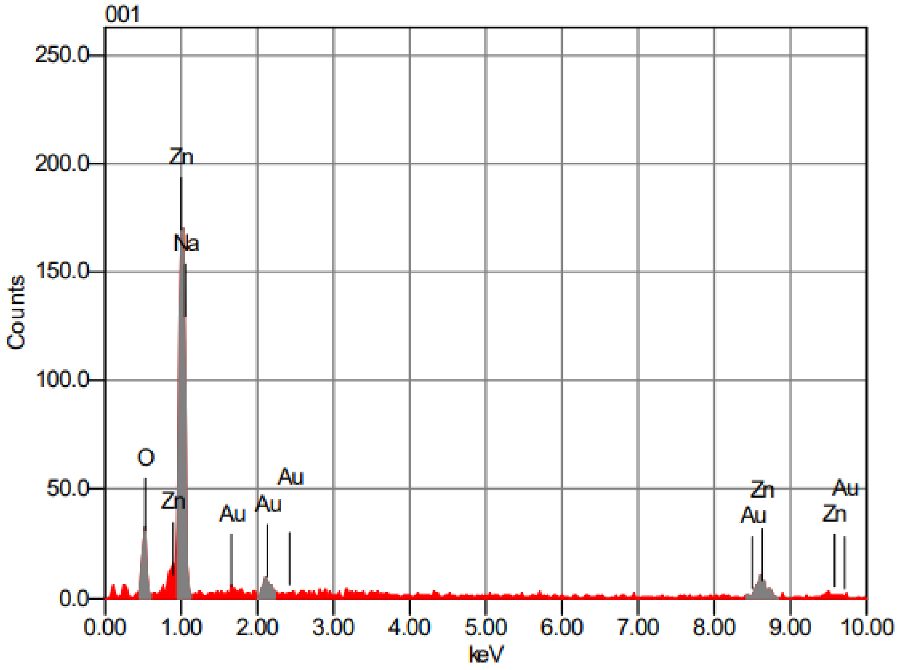

Fig. 3. EDS spectrum of the ZnO/Au thin films.

The absorption spectrum of the ZnO/Au thin films is shown in Fig. 4. A clear absorption edge in the 380 nm wavelength region can be assigned to the band to band absorption of ZnO [18]. Another broad and small peak at around 600 nm was observed, which can be assigned to the plasmon resonance absorption of Au nanoparticles on ZnO thin films.

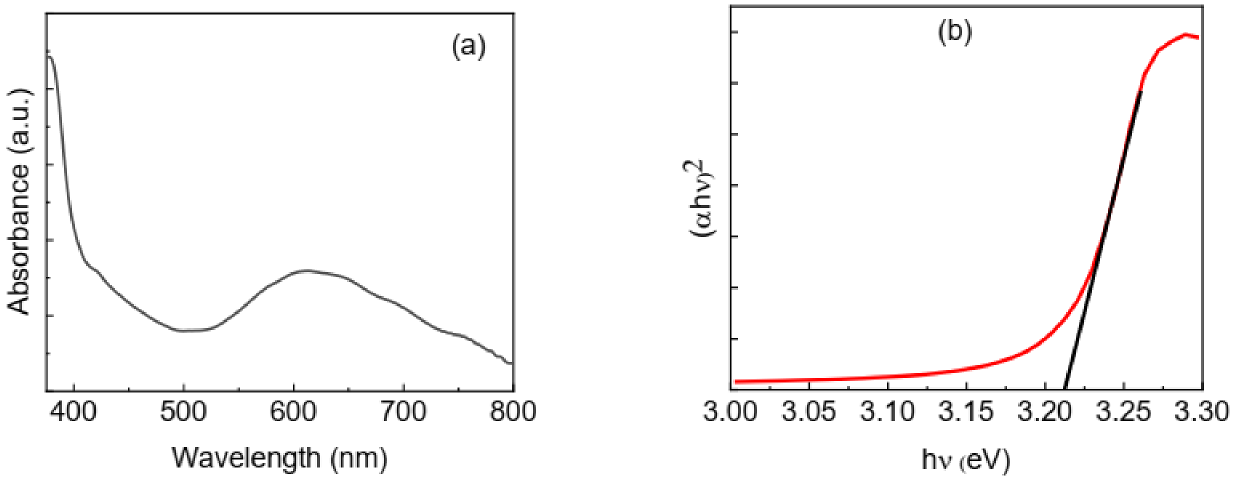

Fig. 4. (a) Absorption spectrum of the ZnO/Au thin films; (b) Tauc plot of the ZnO /Au thin films

The bandgap of the obtained ZnO nanorods was estimated using Tauc's plot method. The energy dependent absorption coefficient of direct semiconductor can be expressed by:

$$\alpha h\nu = A\left(h\nu - E_g\right)^{1/2},$$

where $h\nu$ is the energy of the incoming photon and E_g is the bandgap of the direct semiconductor. By extrapolating the linear part of the $\left(\alpha h\nu\right)^2$ vs. $h\nu$ plot (Fig. 4b) to the energy axis, the bandgap of ZnO nanorods was estimated to be 3.22 eV. It should be noted that this bandgap energy is smaller than that of the UV source used for the PIERS investigation, which will be discussed later.

Raman spectra of 10^{-6} M MB deposited on the ZnO/Au thin film shows characteristic peaks of MB at 803, 895, 1027; 1295, 1388, 1427 cm^{-1} and 1622 cm^{-1}, Fig. 5.

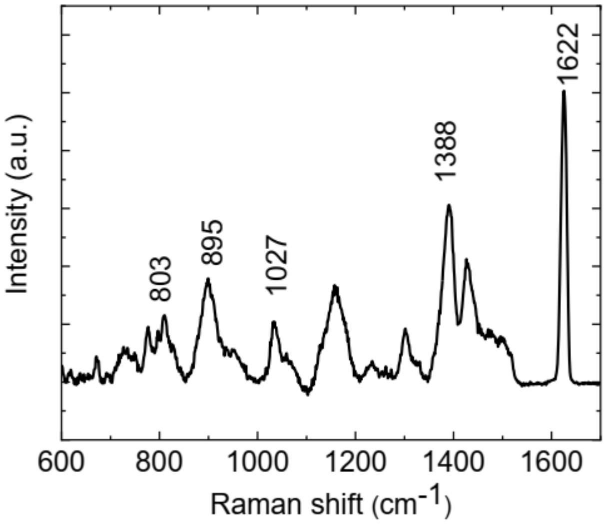

Fig. 5. SERS spectra of MB measured on ZnO/Au thin films.

The uniformity of the sample was demonstrated by the consistence of the spectra measured at 20 random points on the sample, Fig. 6. The spectra (Fig. 6) show high consistency with a low relative standard deviation (RSD) of 7.9 % estimated from the peak intensity at 1622 cm^{-1}. The small RSD implied the uniformity of the gold nanoparticles prepared on the ZnO thin film. The uniformity of the substrate guarantees the highly reproducible signal of Raman probe over the SERS active area, which is critical for quantitative applications based on SERS.

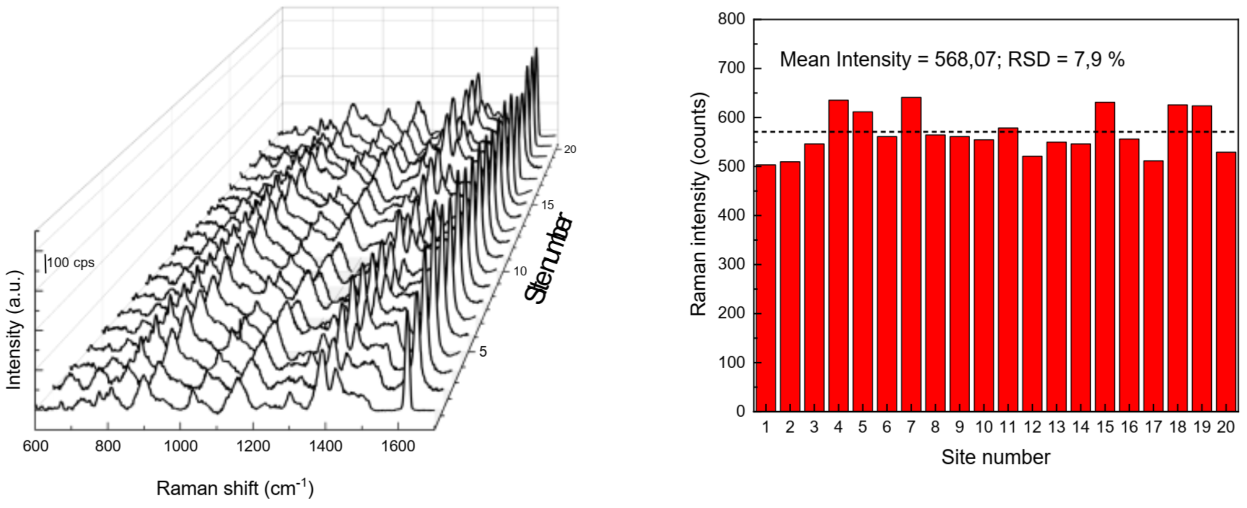

Fig. 6. (a) Raman spectra of 10^{-6} M MB on ZnO/Au thin film measured at 20 random points on the

sample; (b) Raman intensity of the 1622 cm-1 peak measured at the 20 random points

Fig. 7 exhibits the SERS and PIERS spectra of MB (10^{-6} M) on the ZnO/Au substrate. It is found that Raman intensity is significantly enhanced under in situ UV irradiation during measurement. Hence, the PIERS enhancement on ZnO/Au heterogenous thin films can be ascribed to the UV irradiation. The intensity difference of PIERS and SERS spectra clearly demonstrate that a remarkable PIERS enhancement has been achieved via UV excitation. Detailed analysis shows that the enhancement factors of 1622; 1388; 1295; 952; and 895 cm^{-1} peaks of MB are 5.5; 1.87; 2.6; 3.2; 1.78 , respectively.

The mechanism of PIERS in literature is normally attributed to the formation of oxygen vacancies in the semiconductor oxide under deep UV treatment for a long time prior to the Raman measurement [14,15,19]. Such long treatment up to several hours is necessary for the generation of oxygen vacancies at densities high enough for a clear Raman enhancement.

In our experimental setup, the PIERS effect was observed under in situ UV excitation, where the sample was only excited by UV source for several tens of seconds during the Raman measurement. Therefore, we believe that the main reason for the additional enhancement of SERS under UV radiation should not be related to oxygen vacancies formation. Instead, the generation of electron-holes pairs and charge separation due to the heterojunction between ZnO and Au (schottky barrier) is likely responsible for the observed PIERS effect.

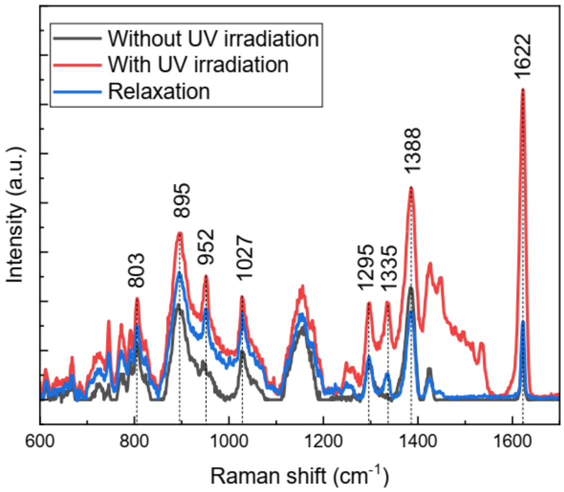

Fig. 9. Raman spectra of MB measured on ZnO/Au thin films () before (black) , under insitu (red) and after (blue) UV excitation.

To further confirm the hypothesis, we performed additional measurements to observe the relaxation of the Raman signal after removing the UV excitation. Raman spectra were collected every 20 s before, during, and after UV excitation being shut down. Raman spectra were collected at the same point in all the measurement to clearly reveal the contribution of each factor.

According to G. Barbillon [20], if the enhancement due to UV excitation is mainly attributed to oxygen vacancies, the signal should decay following an exponential function after removing UV excitation, due to the healing of oxygen vacancies [20]. In our study, we observed a variation of the intensity of the peak at 1622 cm^{-1} upon time once the UV source is removed, Fig. 10. However, as can be observed , the Raman intensity relaxed instantly to the initial value before UV excitation. This result helps to exclude the enhanced mechanism related to oxygen vacancies in our case.

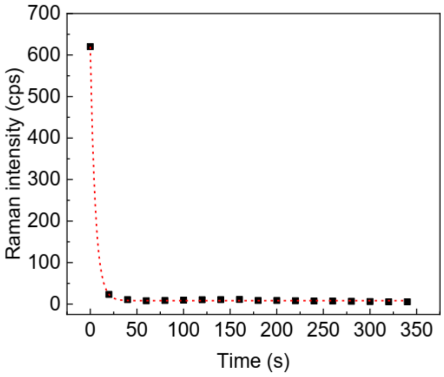

Fig. 10. Intensity of the 1622 cm^{-1} Raman peak after stoping UV excitation.

To better understand the origin of the PIERS effect in this study, we also studied the absorption spectra of the ZnO/Au thin films before UV irradiation, during and after UV irradiation. The results are presented in Fig. 10. The spectra show a clear absorption edge related to band to band transition of ZnO materials at 380 nm and a broad peak at around 600 nm, which can be ascribed to plasmon resonance of Au nanoparticles.

Under UV irradiation, the plasmon peak of Au showed a blue shift of 15 nm. The blueshift can be understood as a result of charge transfer from ZnO to Au. Charge transfer process alters the electron concentration in Au nanostructures, which in turn modify the surface plasmon resonance frequency in Au nanostructures. Shutting down the UV excitations leads to the relaxation to the initial resonance wavelength before UV treatment. The relative increasing electron density in the Au nanoparticles can be estimated by using the expression suggested by Mulvaney et al[21].

$$\frac{\Delta N}{N} = -\frac{2\Delta\lambda}{\lambda_{plasmon}}$$

where N is the electron concentration, $\Delta\lambda$ is the plasmon resonance shift and λ_{plasmon} is the position of the plasmon resonance peak without UV irradiation (λ_{plasmon}= 645 nm). The estimated increase of electron concentration is 5%.

It is noteworthy that the blueshift of the plasmon resonance peak was not observed for Au nanostructures on bare sodalime glass (Fig. 11). The data suggested the important role of ZnO in PIERS effects and further confirm the charge transfer mechanism from ZnO to Au nanoparticles in our case.

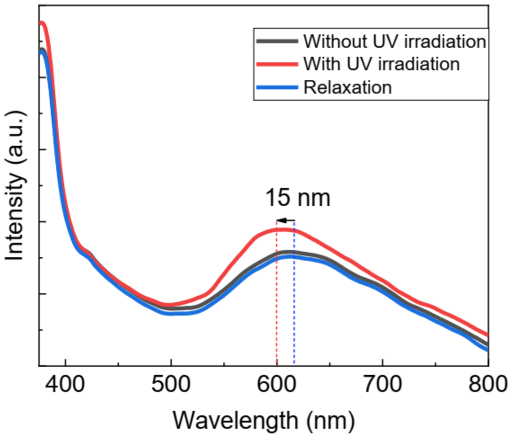

Fig. 11. Absorption spectra of ZnO/Au thin films before irradiation (black), during (red) and after UV irradiation (blue)

The enhancement mechanism of PIERS effect on ZnO/Au thin films can be summarized as following: first, UV excitation with energy greater than the band gap facilitates the generation of electrons and holes in the ZnO semiconductor. In the second step, charge migration occurs at the interface of ZnO and Au. Hot electrons in Au nanostructures can be transferred to the analytes and enhance the Raman signal via chemical mechanism. Simultaneously, tunning surface plasmon resonance frequency in Au nanostructures also contributes to intensification of the Raman scattering. The synergetic enhancement by electromagnetic and chemical mechanism gives rise to the high enhancement of the ZnO/Au thin films.

In this study, to further understand the mechanism of the PIERS effect, we performed simulations of the distribution of the electric field intensity (EM), the enhancement factor (EF), and the shift of plasmon resonance peak of Au nanostructures in the absorption spectrum upon UV excitation by finite difference time domain method (FDTD) using the commercial software "Ansys Lumerical"[22–26]. The used model consists of a spherical Au particle with diameter of 60 nm on a ZnO thin film with a thickness of 200 nm. Real and imaginary part data of the dielectric constant values of Au used in our simulation was extracted from the experiments of Johnson and Christy [27,28]. On the other hand, the real and imaginary data dielectric constant of ZnO materials are obtained from the studies of Christian Stelling et al [29]. The relative refractive index of the surrounding environment is set at 1.0 because the actual environment during experiment is air. Total Field Scatter Field (TFSF) sources used in the simulation include two sources: one represents the excitation laser with a wavelength of 632.8 nm, and the other source is the UV excitation source with a wavelength of 365 nm. The two sources were placed in a container that irradiated perpendicularly to the ZnO/Au material. Finally, the perfectly matched layer (PML) boundary is used to calculate the absorption cross-section[30,31].

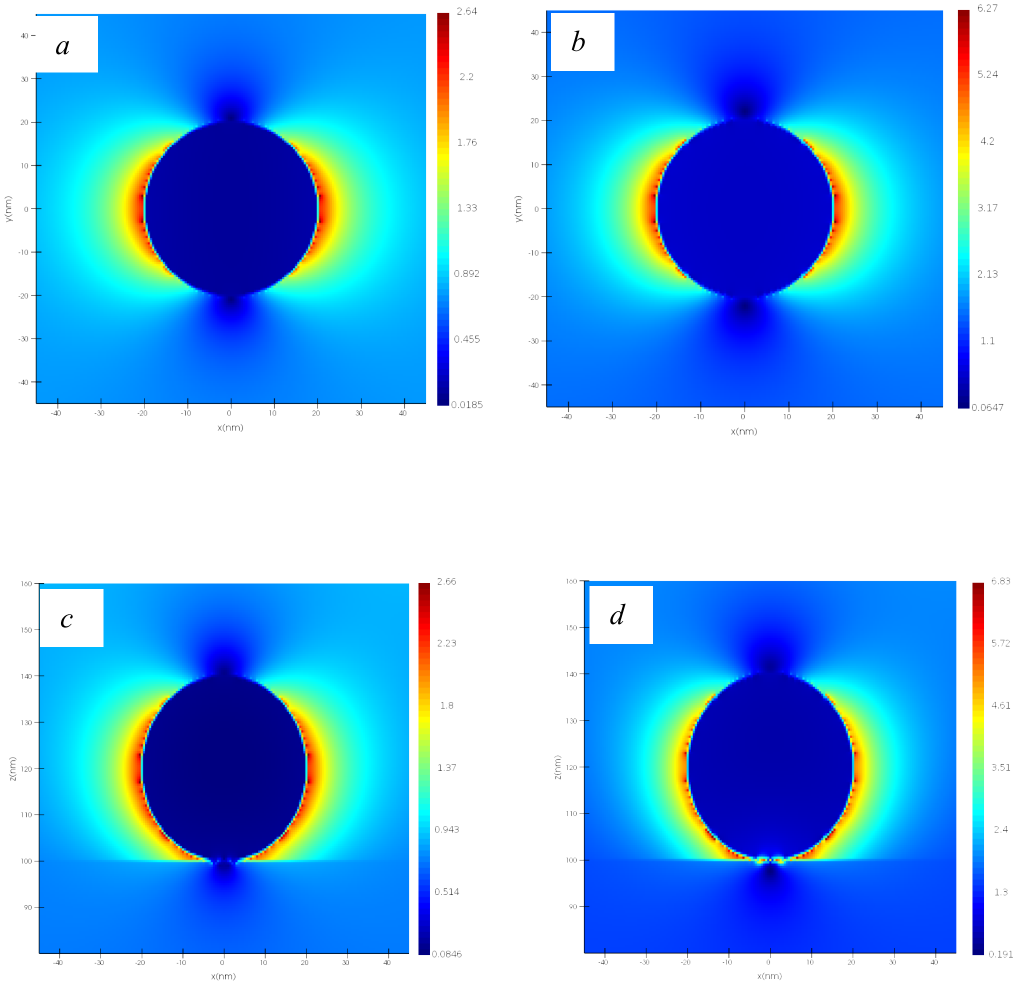

Fig. 12. Spatial distribution of the electric field in the XY plane of ZnO/Au thin films excited by: a) 632.8 nm source, (b) under simultaneous excitation of 632.8 and 365 nm sources. Spatial distribution of the electric field in the XZ plane of ZnO/Au thin films excited by: c) 632.8 nm source, (d) under simultaneous excitation of 632.8 and 365 nm UV sources.

The normalized EM electric field strength $(\frac{|E|^2}{|E_0|^2})$ simulated in the cross-section of ZnO/Au thin film under excitation by a laser source with a wavelength of 632.8 nm is 2.64 (Fig.12a). The enhancement increased nearly 2.6 times to 6.27 when UV excitation is applied simultaneously (Fig. 12b). To further elucidate the charge transfer mechanism between ZnO and Au as discussed in the experimental results, we also performed calculation to obtain the absorption spectrum of ZnO/Au thin films with and without UV excitation.

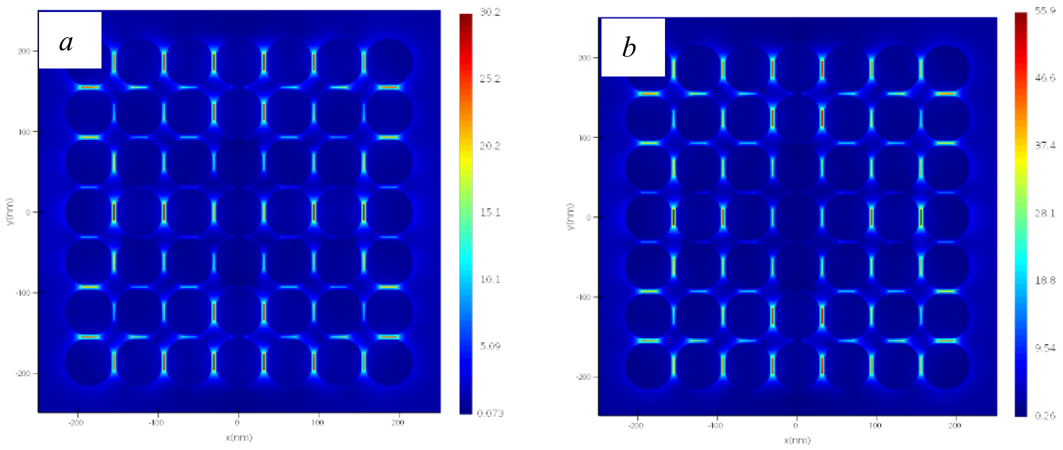

Fig. 13. Spatial distribution of the electric field in the XY plane of the Au nanoparticles on the ZnO substrate excited by: a) 632.8 nm source, (b) 632.8 and 365 nm UV sources.

Simulations data for arrays of Au nanoparticles on ZnO substrates also show that the electric field strength increases after UV excitation combined with the formation of "hot spots" between Au nanoparticles, leading to higher electric intensity, Fig. 13.

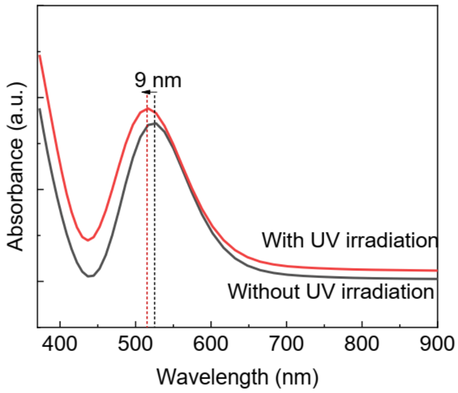

Fig. 14. FDTD simulationof the the UV-Vis absorption cross-section of ZnO, Au, and ZnO/Au before and after UV excitation.

The results in Fig. 14 clearly show the 525 nm peak in the spectrum of ZnO/Au thin film, which can be assigned to the plasmon resonance of the Au nanoparticle. The simulation also shows that the application of the UV excitation leads to a shift of the plasmon resonance peak of the Au nanoparticles on ZnO thin film. The redshift of 9 nm is in good agreement with the experimental absorption data of ZnO/Au nanostructures. The simulation data further strengthens our argument for electron-hole pair generation and charge transfer mechanism of PIERS effect in our case.

Even though PIERS can help to increase Raman intensity, its benefit can not be seen clearly without proof of the ability to lower the detection limit of the analytes. Fig. 15 shows the SERS spectra of MB measured on ZnO/Au thin films with different concentrations, from 10^{-6} M down to 10^{-10} M. The results show that when the analyte concentration decreases gradually, the Raman intensity of characteristic peaks decreases accordingly. The limit of detection of MB measured on ZnO/Au thin films without UV irradiation is 10^{-9} M. At concentrations of 10^{-10} M, the characteristic peaks are almost indistinguishable from the background spectrum. However, when in situ UV treatment is applied during Raman measurement, the characteristic peaks of MB at 1388 and1622 cm^{-1} can be seen clearly. This result shows that the detection limit can be lower by an order of magnitude with simple UV excitation during Raman measurement and also demonstrates the advantage of the PIERS in chemical analysis.

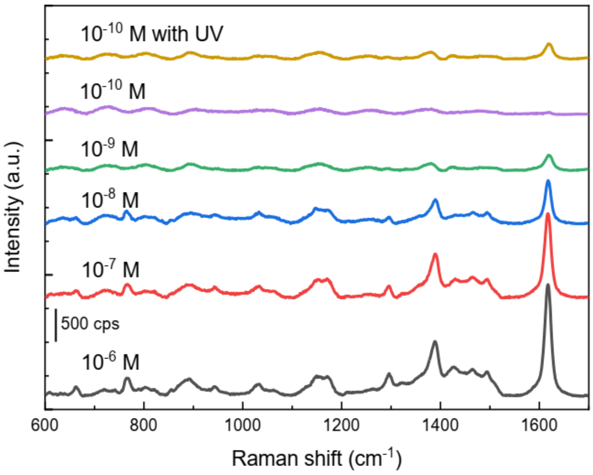

Fig. 15. Raman spectra of MB at different concentrations from 10^{-6} M down to 10^{-10} M measured on ZnO/Au thin films without and with UV irradiation.

4 . Conclusion

In this study, we successfully fabricated a highly crystalline ZnO thin film decorated with Au nanoparticles by the sputtering technique, which can serve as a sensitive SERS substrate. We also demonstrate that Raman signal can be significantly further enhanced up to 5.5 times by in situ UV excitation. The study supports that the enhancement mechanism is mainly due to electron-hole generation and charge separation at the heterojunction of ZnO and Au.

Our study suggests that a UV LED can be conveniently integrated with Raman spectrometer for efficiently improving Raman signal of molecules. Such facile experimental setup is potential for on field analysis applications in various field such as environment monitoring, food safety, biological analysis, etc.

Acknowledgements:

This research is funded by the Vietnam Ministry of Education and Training under grant number B2023-MDA-01. O. Martínez thanks the financial support of the Regional Government of Castilla y León (Junta de Castilla y León) and of the Ministry of Science and Innovation and the European Union NextGenerationEU / PRTR under the project “Programa Complementario de Materiales Avanzados”.

References

[1] Y. Jiang, D.W. Sun, H. Pu, Q. Wei, Surface enhanced Raman spectroscopy (SERS): A novel reliable technique for rapid detection of common harmful chemical residues, Trends Food Sci Technol. 75 (2018) 10–22. https://doi.org/10.1016/J.TIFS.2018.02.020.

[2] M.S.S. Bharati, V.R. Soma, Flexible SERS substrates for hazardous materials detection: recent advances, Opto-Electronic Advances, Vol. 4, Issue 11, Pp. 210048-1 - 210048-26. 4 (2021) 210048–1. https://doi.org/10.29026/OEA.2021.210048.

[3] J. Langer, D.J. de Aberasturi, J. Aizpurua, R.A. Alvarez-Puebla, B. Auguié, J.J. Baumberg, G.C. Bazan, S.E.J. Bell, A. Boisen, A.G. Brolo, J. Choo, D. Cialla-May, V. Deckert, L. Fabris, K.

Faulds, F. Javier García de Abajo, R. Goodacre, D. Graham, A.J. Haes, C.L. Haynes, C. Huck, T. Itoh, M. Käll, J. Kneipp, N.A. Kotov, H. Kuang, E.C. Le Ru, H.K. Lee, J.F. Li, X.Y. Ling, S.A. Maier, T. Mayerhöfer, M. Moskovits, K. Murakoshi, J.M. Nam, S. Nie, Y. Ozaki, I. Pastoriza-Santos, J. Perez-Juste, J. Popp, A. Pucci, S. Reich, B. Ren, G.C. Schatz, T. Shegai, S. Schlücker, L.L. Tay, K. George Thomas, Z.Q. Tian, R.P. van Duyne, T. Vo-Dinh, Y. Wang, K.A. Willets, C. Xu, H. Xu, Y. Xu, Y.S. Yamamoto, B. Zhao, L.M. Liz-Marzán, Present and future of surface-enhanced Raman scattering, ACS Nano. 14 (2020) 28–117. https://doi.org/10.1021/acsnano.9b04224.

[4] S.-Y. Ding, X.-M. Zhang, B. Ren, Z.-Q. Tian, Surface-Enhanced Raman Spectroscopy (SERS): General Introduction, Encyclopedia of Analytical Chemistry. (2014) 1–34. https://doi.org/10.1002/9780470027318.A9276.

[5] J. Zhao, Z. Wang, J. Lan, I. Khan, X. Ye, J. Wan, Y. Fei, S. Huang, S. Li, J. Kang, Recent advances and perspectives in photo-induced enhanced Raman spectroscopy, Nanoscale. 13 (2021) 8707–8721. https://doi.org/10.1039/D1NR01255J.

[6] V.T. Tran, T.H. Tran, M.P. Le, N.H. Pham, V.T. Nguyen, D.B. Do, X.T. Nguyen, B.N.Q. Trinh, T.T. Van Nguyen, V.T. Pham, M.Q. Luu, A.B. Ngac, Highly efficient photo-induced surface enhanced Raman spectroscopy from ZnO/Au nanorods, Opt Mater (Amst). 134 (2022) 113069. https://doi.org/10.1016/J.OPTMAT.2022.113069.

[7] S. Cong, X. Liu, Y. Jiang, W. Zhang, Z. Zhao, Surface Enhanced Raman Scattering Revealed by Interfacial Charge-Transfer Transitions, The Innovation. 1 (2020) 100051. https://doi.org/10.1016/J.XINN.2020.100051.

[8] C. Wang, X. Guo, Q. Fu, TiO2 Thickness-Dependent Charge Transfer in an Ordered Ag/TiO2/Ni Nanopillar Arrays Based on Surface-Enhanced Raman Scattering, Materials. 15 (2022). https://doi.org/10.3390/MA15103716.

[9] M. Zhang, H. Sun, X. Chen, J. Yang, L. Shi, T. Chen, Z. Bao, J. Liu, Y. Wu, Highly Efficient Photoinduced Enhanced Raman Spectroscopy (PIERS) from Plasmonic Nanoparticles Decorated 3D Semiconductor Arrays for Ultrasensitive, Portable, and Recyclable Detection of Organic Pollutants, ACS Sens. 4 (2019) 1670–1681. https://doi.org/10.1021/acssensors.9b00562.

[10] A. Brognara, B.R. Bricchi, L. William, O. Brinza, M. Konstantakopoulou, A.L. Bassi, M. Ghidelli, N. Lidgi-Guigui, New Mechanism for Long Photo-Induced Enhanced Raman Spectroscopy in Au Nanoparticles Embedded in TiO2, Small. 18 (2022) 2201088. https://doi.org/10.1002/SMLL.202201088.

[11] S. Almohammed, F. Zhang, B.J. Rodriguez, J.H. Rice, Photo-induced surface-enhanced Raman spectroscopy from a diphenylalanine peptide nanotube-metal nanoparticle template, Scientific Reports 2018 8:1. 8 (2018) 1–10. https://doi.org/10.1038/s41598-018-22269-x.

[12] G. Barbillon, T. Noblet, C. Humbert, Highly crystalline ZnO film decorated with gold nanospheres for PIERS chemical sensing, Physical Chemistry Chemical Physics. 22 (2020) 21000–21004. https://doi.org/10.1039/d0cp03902k.

[13] G. Barbillon, Au Nanoparticles Coated ZnO Film for Chemical Sensing by PIERS Coupled to SERS, Photonics. 9 (2022). https://doi.org/10.3390/photonics9080562.

[14] D. Glass, R. Quesada-Cabrera, S. Bardey, P. Promdet, R. Sapienza, V. Keller, S.A. Maier, V. Caps, I.P. Parkin, E. Cortés, Probing the Role of Atomic Defects in Photocatalytic Systems through Photoinduced Enhanced Raman Scattering, ACS Energy Lett. 6 (2021) 4273–4281. https://doi.org/10.1021/acsenergylett.1c01772.

[15] D. Glass, E. Cortés, W.J. Peveler, C.R. Howle, R. Quesada-Cabrera, I.P. Parkin, S.A. Maier, Enhancing hybrid metal-semiconductor systems beyond SERS with PIERS (photo-induced enhanced Raman scattering) for trace analyte detection, 1141602 (2020) 2. https://doi.org/10.1117/12.2557517.

[16] D. Glass, E. Cortés, S. Ben-Jaber, T. Brick, W.J. Peveler, C.S. Blackman, C.R. Howle, R. Quesada-Cabrera, I.P. Parkin, S.A. Maier, Dynamics of Photo-Induced Surface Oxygen Vacancies in Metal-Oxide Semiconductors Studied Under Ambient Conditions, Advanced Science. 6 (2019). https://doi.org/10.1002/advs.201901841.

[17] Q.K. Doan, M.H. Nguyen, C.D. Sai, V.T. Pham, H.H. Mai, N.H. Pham, T.C. Bach, V.T. Nguyen, T.T. Nguyen, K.H. Ho, T.H. Tran, Enhanced optical properties of ZnO nanorods decorated with gold nanoparticles for self cleaning surface enhanced Raman applications, Appl Surf Sci. 505 (2020) 144593. https://doi.org/10.1016/J.APSUSC.2019.144593.

[18] J. Phelipot, N. Ledos, T. Dombray, M.P. Duffy, M. Denis, T. Wang, Y. Didane, M. Gaceur, Q. Bao, X. Liu, M. Fahlman, P. Delugas, A. Mattoni, D. Tondelier, B. Geffroy, P.A. Bouit, O. Margeat, J. Ackermann, M. Hissler, Highly Emissive Layers based on Organic/Inorganic Nanohybrids Using Aggregation Induced Emission Effect, Adv Mater Technol. 7 (2022).

https://doi.org/10.1002/admt.202100876.

[19] J. Zhao, Z. Wang, J. Lan, I. Khan, X. Ye, J. Wan, Y. Fei, S. Huang, S. Li, J. Kang, Recent advances and perspectives in photo-induced enhanced Raman spectroscopy, Nanoscale. 13 (2021) 8707–8721. https://doi.org/10.1039/D1NR01255J.

[20] G. Barbillon, Oxygen vacancy dynamics in highly crystalline zinc oxide film investigated by piers effect, Materials. 14 (2021). https://doi.org/10.3390/ma14164423.

[21] P. Mulvaney, J. Pérez-Juste, M. Giersig, L.M. Liz-Marzán, C. Pecharromán, Drastic surface plasmon mode shifts in gold nanorods due to electron charging, Plasmonics. 1 (2006) 61–66. https://doi.org/10.1007/S11468-005-9005-0.

[22] N. Yamamoto, S. Ohtani, F.J. García De Abajo, Gap and mie plasmons in individual silver nanospheres near a silver surface, Nano Lett. 11 (2011) 91–95. https://doi.org/10.1021/nl102862x.

[23] Z.L. Yang, Q.H. Li, F.X. Ruan, Z.P. Li, B. Ren, H.X. Xu, Z.Q. Tian, FDTD for plasmonics: Applications in enhanced Raman spectroscopy, Chinese Science Bulletin. 55 (2010) 2635–2642. https://doi.org/10.1007/s11434-010-4044-0.

[24] I. Ahmed, E.H. Khoo, O. Kurniawan, E.P. Li, Modeling and simulation of active plasmonics with the FDTD method by using solid state and Lorentz–Drude dispersive model, Journal of the Optical Society of America B. 28 (2011) 352. https://doi.org/10.1364/josab.28.000352.

[25] V. Shvalya, G. Filipič, J. Zavašnik, I. Abdulhalim, U. Cvelbar, Surface-enhanced Raman spectroscopy for chemical and biological sensing using nanoplasmonics: The relevance of interparticle spacing and surface morphology, Appl Phys Rev. 7 (2020). https://doi.org/10.1063/5.0015246.

[26] S.Y. Wang, X.X. Jiang, T.T. Xu, X.P. Wei, S.T. Lee, Y. He, Reactive ion etching-assisted surface-enhanced Raman scattering measurements on the single nanoparticle level, Appl Phys Lett. 104 (2014). https://doi.org/10.1063/1.4884060.

[27] P.B. Johnson, R.W. Christy, Optical Constants of the Noble Metals, Phys Rev B. 6 (1972) 4370. https://doi.org/10.1103/PhysRevB.6.4370.

[28] E.D. Palik, ed., Handbook of Optical Constants of Solids I-III, (1998).

[29] C. Stelling, C.R. Singh, M. Karg, T.A.F. König, M. Thelakkat, M. Retsch, Plasmonic nanomeshes: their ambivalent role as transparent electrodes in organic solar cells, Sci Rep. 7 (2017). https://doi.org/10.1038/SREP42530.

[30] W. Wang, J. Zhang, Y. Zhang, Z. Xie, G. Qin, Optical absorption enhancement in submicrometre crystalline silicon films with nanotexturing arrays for solar photovoltaic applications, J Phys D Appl Phys. 46 (2013) 195106. https://doi.org/10.1088/0022-3727/46/19/195106.

[31] T. Badloe, I. Kim, J. Rho, Biomimetic ultra-broadband perfect absorbers optimised with reinforcement learning, Physical Chemistry Chemical Physics. 22 (2020) 2337–2342. https://doi.org/10.1039/C9CP05621A.